Enhanced pyroelectric properties of Bi$_{1-x}$La$_x$FeO$_3$ thin films

Lei Zhang (iD), Yen-Lin Huang, Gabriel Velarde, Anirban Ghosh, Shishir Pandya, David Garcia, Ramamoorthy Ramesh, and Lane W. Martin (iD)

View Online   Export Citation   CrossMark

Enhanced pyroelectric properties of Bi₁₋ₓLaₓFeO₃ thin films

View Online   Export Citation   CrossMark

Lei Zhang,[1,2] (ID) Yen-Lin Huang,[2] Gabriel Velarde,[1] Anirban Ghosh,[1] Shishir Pandya,[1] David Garcia,[1] Ramamoorthy Ramesh,[1,2] and Lane W. Martin[1,2,a)] (ID)

AFFILIATIONS

[1] Department of Materials Science and Engineering, University of California, Berkeley, California 94720, USA
[2] Materials Sciences Division, Lawrence Berkeley National Laboratory, Berkeley, California 94720, USA

[a)] Author to whom correspondence should be addressed: lwmartin@berkeley.edu

ABSTRACT

There is growing interest in the study of thin-film pyroelectric materials because of their potential for high performance thermal-energy conversion, thermal sensing, and beyond. Electrothermal susceptibilities, such as pyroelectricity, are known to be enhanced in proximity to polar instabilities, and this is conventionally accomplished by positioning the material close to a temperature-driven ferroelectric-to-paraelectric phase transition. The high Curie temperature (T_C) for many ferroelectrics, however, limits the utility of these materials at room-temperature. Here, the nature of pyroelectric response in thin films of the widely studied multiferroic Bi₁₋ₓLaₓFeO₃ (x = 0–0.45) is probed. While BiFeO₃ itself has a high T_C, lanthanum substitution results in a chemically induced lowering of the ferroelectric-to-paraelectric and structural-phase transition. The effect of isovalent lanthanum substitution on the structural, dielectric, ferroelectric, and pyroelectric response is investigated using reciprocal-space-mapping studies; field-, frequency-, and temperature-dependent electrical measurements; and phase-sensitive pyroelectric measurements, respectively. While BiFeO₃ itself has a rather small pyroelectric coefficient at room temperature (~−40 μC/m² K), 15% lanthanum substitution results in an enhancement of the pyroelectric coefficient by 100% which is found to arise from a systematic lowering of T_C.

The pyroelectric effect is the variation of the remanent polarization P as a function of temperature T at constant electric field E [parameterized by the pyroelectric coefficient $\pi = (\partial P/\partial T)_E$]. Pyroelectric effects, while long used for thermal sensing/imaging,[1,2] have drawn renewed interest for their potential for efficient low-grade (<100 °C) waste-heat energy conversion.[3–7] Focus on thin-film geometries, in particular, comes from their potential for high-breakdown fields (allowing for increased energy density) and low thermal masses (allowing for faster temperature cycling and thus increased power density).[6,8] In turn, advances in both our understanding of and routes to manipulate π of thin films are essential to ultimately produce such devices. With recent developments in thin-film epitaxy of ferroic materials[9–11] and advances in the direct measurement of thin films,[12,13] researchers have clarified the nature of pyroelectric effects in thin-film materials, including unraveling extrinsic contributions to π that arise from ferroelastic domains and domain walls,[14,15] shoring up the true nature of pyroelectric response in doped hafnium oxide thin films,[16,17] etc.

In general, π is maximized near polar instabilities where phonon-mode softening leads to a temperature-dependent polar-phase transition.[18,19] The enhancement of π can be realized by placing the material close to a temperature-driven ferroelectric-to-paraelectric phase transition; however, T_C far exceeds room temperature for the majority of ferroelectrics, thus limiting the application of this approach.[18,19] To improve π, one can, for example, shift the ferroelectric-to-paraelectric phase transition closer to room-temperature through hydrostatic strain,[20] biaxial strain,[21] or chemical substitution.[22] For example, it is possible to lower T_C via chemical substitution to enhance pyroelectric properties as was illustrated in bulk lanthanum-doped lead zirconate[23] and bulk Ba₁₋ₓSrₓTiO₃.[24] In BiFeO₃, rare-earth isovalent substitution (Bi₁₋ₓReₓFeO₃; Re = La, Nd, Sm, and Gd) can also significantly reduce T_C.[25–32] At the

same time, the piezoelectric coefficient d_{33} can be enhanced (as in $Bi_{1-x}Sm_xFeO_3$).[31] The role of such rare-earth isovalent substitution in controlling the electrothermal susceptibilities has remained unclear, owing to the difficulty in fabricating high-quality $BiFeO_3$,[33] thus motivating the present study.

Here, the $Bi_{1-x}La_xFeO_3$ (x = 0–0.45) system was chosen as a model system for studying chemical substitution-induced phase boundaries at room temperature. Using a combination of advanced thin-film epitaxy, X-ray diffraction, polarization-electric-field measurements, and temperature-dependent dielectric measurements, the position of the chemically driven phase boundary and its effects on properties at room temperature were probed. Microfabricated electrothermal devices were, in turn, used to probe the pyroelectric nature of the various $Bi_{1-x}La_xFeO_3$ heterostructures and revealed that although pure $BiFeO_3$ thin films have a fairly small $\pi \approx -40 \ \mu C/m^2$ K at room-temperature, 15% lanthanum substitution enhances π by ~100%. Reciprocal-space-mapping (RSM) studies confirmed a rhombohedral structure for the $Bi_{1-x}La_xFeO_3$ films with x ≤ 0.15 and thus, that an increase in the pyroelectric response due to polarization rotation can be excluded. The enhancement of π, instead, is found to arise from a systematic lowering of T_C. Overall, this work demonstrates a route toward improving pyroelectric response through isovalent-cation substitution in the $Bi_{1-x}La_xFeO_3$ system and further expands our understanding of and routes to control pyroelectric effects in thin films.

In the bulk, $BiFeO_3$ exhibits an $R3c$ rhombohedrally distorted perovskite structure that undergoes a phase transition from a cubic-paraelectric phase to a ferroelectric-rhombohedral phase at $T_C \approx 1103$ K resulting in a robust spontaneous polarization ($\approx 100 \ \mu C/cm^2$) along the $\langle 111 \rangle$.[34–36] While $BiFeO_3$ has one of the highest reported remanent polarization values, its near-room-temperature pyroelectric properties remained largely unexplored in any form, but especially in thin films, due to a lack of high-quality materials.[33,37–40] Electrical leakage—arising from both a smaller bandgap as compared to other polar, ferroelectric materials and

difficulty in controlling the chemistry and defect structures in this material—makes direct measurements of π challenging at best. For example, both cation and anion nonstoichiometry, in part due to the volatility of species like bismuth during synthesis, can result in an increased concentration of free carriers and electrical leakage[27,41] which can also hamper low-frequency ferroelectric performance.[42]

60 nm $SrRuO_3$/150 nm $Bi_{1-x}La_xFeO_3$ (x = 0.05, 0.10, 0.15, 0.27, and 0.45)/30 nm $SrRuO_3$ heterostructures wherein the $SrRuO_3$ serves as the top and bottom electrodes were grown on (110)-oriented, single-crystalline $DyScO_3$ substrates by pulsed-laser deposition using a KrF excimer laser (248 nm, ComPex Pro 205F, Coherent, Inc.). The bottom $SrRuO_3$ was grown in a dynamic oxygen pressure of 100 mTorr, at a growth temperature of 700 °C, a repetition rate of 15 Hz, and a laser fluence of 1.0 J/cm². After that, $Bi_{1-x}La_xFeO_3$ was grown at the same temperature and oxygen pressure, a repetition rate of 15 Hz, and a laser fluence of 1.5 J/cm². Finally, the top $SrRuO_3$ was grown under the same condition as of the bottom $SrRuO_3$. Following growth, the samples were cooled to room temperature at a cooling rate of 5 °C/min under a static oxygen pressure of 760 Torr. A high-resolution X-ray diffractometer with a Cu source (X'Pert³ MRD, Panalytical) was used to perform line scans and RSM studies. Ferroelectric polarization hysteresis loops were measured using a Precision Multiferroic Tester (Radiant Technologies, Inc.). Measurements were completed on symmetric capacitor structures using $SrRuO_3$ top and bottom electrodes at a frequency of 10 kHz. Temperature- and electric-field-dependent low-field permittivity and loss tangent were measured using an impedance analyzer (Keysight E4990A) using an ac excitation field of 1.3 kV/cm as a function of frequency. The trilayers synthesized by pulsed-laser deposition were patterned using standard photolithography and ion milled to define the ferroelectric capacitor [Fig. 1(a)]. The top $SrRuO_3$ electrode layer and the $Bi_{1-x}La_xFeO_3$ ferroelectric layer were then ion milled to expose the bottom $SrRuO_3$ electrode layer after a second photolithography step. Following that, a 200-nm-thick blanket layer of SiN_x was deposited using
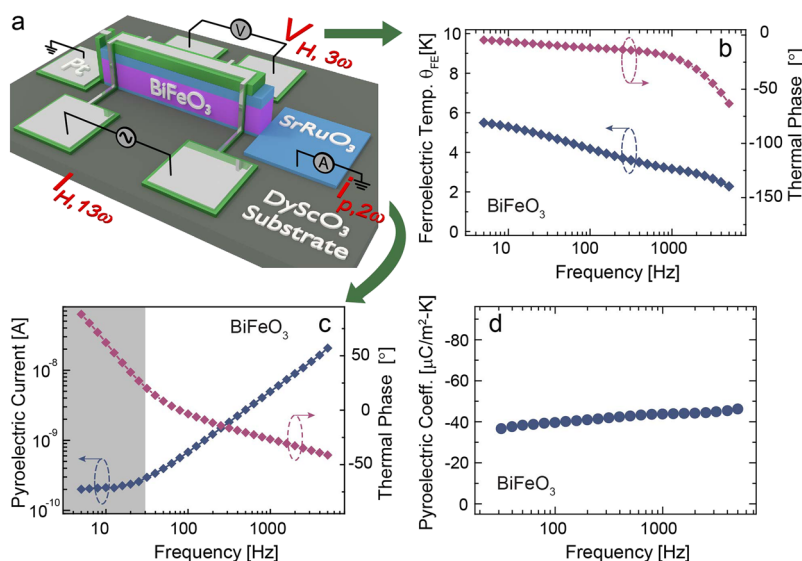
FIG. 1. (a) A schematic illustration of the device structure wherein ac current at frequency ω is applied to the platinum heater line on top of the $BiFeO_3$ thin film that is sandwiched by $SrRuO_3$ electrodes resulting in a pyroelectric current at the frequency of 2ω collected by the bottom electrode. (b) Temperature oscillation (θ_{FE}, left axis) and thermal phase (right axis) in the ferroelectric layer are measured by the voltage at a frequency of 3ω using the 3ω method as a function of heating current frequency (ω). (c) Pyroelectric current (left axis) and thermal phase (right axis) for the $BiFeO_3$ heterostructures as a function of heating current frequency at zero dc bias (the gray area denotes a regime wherein spurious in-phase current is prevalent; it is found to significantly increase as the frequency of measurement decreases). (d) Pyroelectric coefficient of $BiFeO_3$ heterostructures as a function of heating current frequency at zero dc bias.

plasma-enhanced chemical vapor deposition (SiH_4 + NH_3 based). The SiN_x was then selectively etched using reactive-ion etching (using a CHF_3 and O_2 plasma). Finally, a 100-nm-thick platinum layer with a 1-nm-thick tantalum adhesion layer was sputtered to define the thermal heating and sensing circuit (with a four-point probe design for sourcing current and sensing voltage and providing contact pads). The locally oscillated temperature at a frequency of 2ω was generated by driving a sinusoidal heating current (Keithley 6221 current source) with a magnitude of 10 mA (rms) at the desired frequency of 1ω across the top platinum heater line. The magnitude and phase of the temperature of the platinum heater line are calculated using the 3ω method with a custom-designed electrical circuit, and the temperature of the ferroelectric layer is calculated by solving a one-dimensional thermal transport model.[12] The devices were poled using a Precision Multiferroic Tester (Radiant Technologies, Inc.), and the pyroelectric current was measured with the polarization of the ferroelectric in both the up-poled and down-poled states. The total current at the frequency of 2ω due to the sinusoidal heating is measured via a phase-sensitive detection using a lock-in amplifier (Stanford Research SR830), and the pyroelectric current is extracted from the out-of-phase component of total measured current with the temperature oscillation.[12]

Studies here focus on 60 nm $SrRuO_3$/150 nm $Bi_{1-x}La_xFeO_3$ (x = 0, 0.10, 0.15, 0.27, and 0.45)/30 nm $SrRuO_3$/$DyScO_3$ (110) heterostructures wherein the $SrRuO_3$ serves as the top and bottom electrodes for subsequent dielectric, ferroelectric, and pyroelectric measurements. All films were grown via pulsed-laser deposition following established procedures.[42,43] Electrothermal measurement devices [Fig. 1(a)], with both *in situ* heating and temperature-sensing capabilities, were fabricated following established procedures.[12] Focusing initially on $BiFeO_3$ heterostructures to establish a baseline of device operation and function, a sinusoidal heating current of 10 mA (rms) with various frequencies (f = 5–5000 Hz) was applied on a platinum heater line generating a periodically oscillating temperature at a frequency of 2f within the $BiFeO_3$

heterostructures, the magnitude of which is measured by the 3ω method[12] [Fig. 1(b)]. The resulting pyroelectric current [i_p, ideally 90° out-of-phase with the 2ω ($\omega = 2\pi f$) temperature signal] is measured by phase-sensitive detection [Fig. 1(c)]. At low frequencies ($\lesssim$30 Hz), the current in-phase with the 2ω temperature signal (which is indicative of spurious effects, e.g., thermally stimulated currents) is found to increase significantly in the $BiFeO_3$ [shaded area, Fig. 1(c)].[12] Such spurious, thermally stimulated currents, which are nonpyroelectric in nature, are common in ferroelectric materials and arise from detrapping of charge from defects.[44] These currents should not be, and are not, considered in the extraction of π, which was calculated using $\pi = i_p(A\frac{dT}{dt})^{-1}$, where A is the area of the device and dT/dt is the rate of temperature change [Fig. 1(d)]. It should be noted that such thermally stimulated currents are the primary factor leading to the overestimation of π in the literature and are a strong motivator for the application of direct, phase-sensitive measurements noted herein. For the $BiFeO_3$ thin films, π was directly measured to be -43 $\mu C/m^2$ K at 1 kHz.[41] Such a value is lower than the zero-field values measured for other widely studied materials such as $PbZr_{0.2}Ti_{0.8}O_3$ thin films (~-200 $\mu C/m^2$ K),[3] $PbZr_{0.45}Ti_{0.55}O_3$ thin films (~-420 $\mu C/m^2$ K),[45] $0.68Pb(Mg_{1/3}Nb_{2/3})O_3$-$0.32PbTiO_3$ thin films (~-150 $\mu C/m^2$ K),[3] and $LiTaO_3$ (-100 to -200 $\mu C/m^2$ K[46–48]) but is higher than that of silicon-doped HfO_2 (~-20 $\mu C/m^2$ K).[16] Given that the T_C of $BiFeO_3$ (~1103 K) is much higher than that of $PbZr_{0.2}Ti_{0.8}O_3$ (470 K),[3] $0.68Pb(Mg_{1/3}Nb_{2/3})O_3$-$0.32PbTiO_3$ (590 K),[3] and $LiTaO_3$ (890 K)[46] and that $BiFeO_3$ has a rhombohedral structure (such that the polarization points along the $\langle111\rangle$ and, thus, only a fraction of polarization is projected along the out-of-plane capacitor device), the data are self-consistent. The essential question, in turn, is what can be done to further improve the pyroelectric response of $BiFeO_3$?

Having established the baseline pyroelectric response of $BiFeO_3$, we proceeded to explore the evolution of π in the $Bi_{1-x}La_xFeO_3$ system (x = 0, 0.10, 0.15, 0.27, and 0.45) as we approach and transition across the known structural-phase

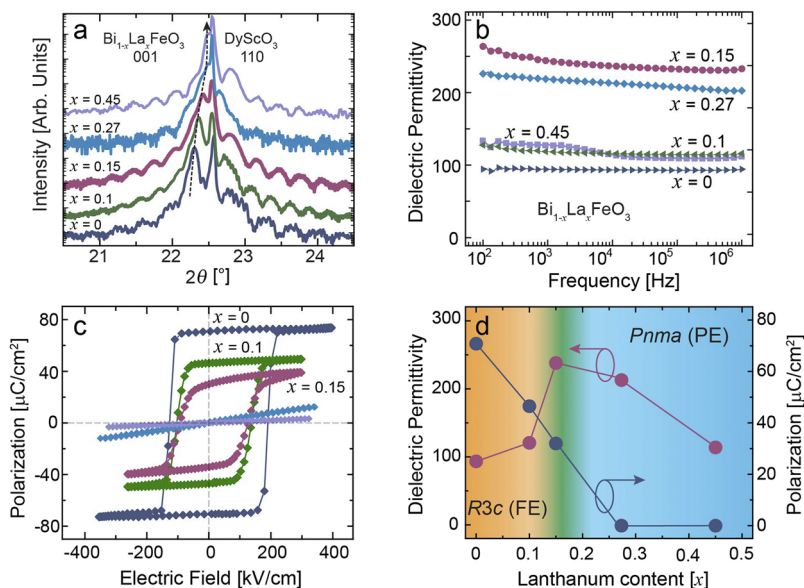**FIG. 2**. (a) X-ray diffraction $\theta-2\theta$ scans revealing high-quality thin films and the contraction of the out-of-plane lattice parameter with increasing lanthanum content (as indicated by the dashed black arrow). (b) Dielectric permittivity (ε_r) as a function of frequency (measured at an ac excitation field of 1.3 kV/cm) and (c) polarization-electric-field hysteresis loops (measured at 10 kHz) for the various $Bi_{1-x}La_xFeO_3$ heterostructures. (d) Summary of the evolution of the dielectric permittivity (ε_r, left axis) and spontaneous polarization (right axis) with lanthanum content (x) in the $Bi_{1-x}La_xFeO_3$ heterostructures.

boundary. Room-temperature X-ray diffraction θ–2θ scans [Fig. 2(a)] reveal that the $Bi_{1-x}La_xFeO_3$ heterostructures are epitaxial and single-phase and that the out-of-plane lattice parameter decreases with increasing lanthanum substitution [black arrow, Fig. 2(a)]. Room-temperature dielectric permittivity [Fig. 2(b) and the supplementary material, Fig. S1(a)] and dielectric loss [supplementary material, Fig. S1(b)] as a function of frequency reveal that the dielectric permittivity increases with lanthanum substitution up to x = 0.15 and then decreases upon further increasing the lanthanum content, consistent with previous findings.[42,49] The dielectric loss reveals that all films have low loss across the frequency regime studied herein, except for in the $Bi_{1-x}La_xFeO_3$ heterostructures with some of the highest lanthanum concentrations (e.g., x = 0.45) where potential signatures of space charge effects arise from substitution-related defects. Ferroelectric hysteresis loops measured using the same symmetric capacitor structures [shown here at 10 kHz, Fig. 2(c)] reveal that the remanent polarization decreases from a maximum of ~70 $\mu C/cm^2$ for BiFeO_3 (consistent with previous reports)[34,36,42] to a value of ~32 $\mu C/cm^2$ for x = 0.15; for x = 0.27 and 0.45, no hysteresis loops were observed as the films are paraelectric. A summary of both the dielectric permittivity and remanent polarization evolution as a function of lanthanum substitution [Fig. 2(d)] at room-temperature suggests the presence of an anomaly near x = 0.15–0.20 corresponding to the likely position of the ferroelectric-to-paraelectric phase transition in $Bi_{1-x}La_xFeO_3$, again consistent with previous reports.[50]

Armed with this knowledge on the location of the structural-phase transition in the $Bi_{1-x}La_xFeO_3$ heterostructures, we proceed to explore how the pyroelectric properties evolve near this boundary. For brevity, we show data on the pyroelectric measurements for the x = 0.15 heterostructures [Fig. 3(a)], but additional data are provided including data for x = 0.1 (supplementary material, Fig. S2) and x = 0.15 (supplementary material, Fig. S3). Similar scaling for temperature oscillations and thermal-phase lag is observed for the x = 0.15 (and other) heterostructures. π, as a function of measurement frequency, for x = 0, 0.10, 0.15, and 0.27 heterostructures are shown together for comparison [Fig. 3(b)]. Little variation in π is seen until the lanthanum content approaches the structural phase boundary wherein, at x = 0.15, π jumps from a value of −43 to −49 $\mu C/m^2$ K (at 10 kHz) for x = 0, 0.1 heterostructures to a value of −85 $\mu C/m^2$ K (at 10 kHz) for x = 0.15 heterostructures. Unsurprisingly, upon transitioning beyond the structural phase boundary into the paraelectric phase, the x = 0.27 heterostructures exhibit no pyroelectric response. The doubling of π upon transitioning from x = 0 to 0.15 is dramatic considering the remanent polarization of the x = 0.15 heterostructure is only about half that of the x = 0 heterostructure.

Such a significant change in the pyroelectric response could result from two possible reasons. First, it could be that the material undergoes a structural transition from rhombohedral to orthorhombic symmetry wherein the polarization direction rotates from the $\langle 111 \rangle$ to the $\langle 001 \rangle$ so that the out-of-plane projection of the polarization increases without having any change in the magnitude of π. Another possible reason is that T_C is reduced with increasing rare-earth substitution. Finally, some combination of the two effects could occur. To fully understand the mechanism for the enhanced pyroelectric response, detailed studies of the evolution of the crystal structure of the various $Bi_{1-x}La_xFeO_3$ heterostructures were completed via RSM studies about the DyScO_3 334- and $Bi_{1-x}La_xFeO_3$ pseudocubic 203_c-diffraction conditions. These diffraction conditions were chosen since they possess in-plane directional information to provide true crystal symmetry. RSM studies for the x = 0 [Fig. 4(a)], 0.10 [Fig. 4(b)], 0.15 [Fig. 4(c)], and 0.27 [Fig. 4(d)] heterostructures indicate that all heterostructures are coherently strained to the DyScO_3 substrates. For the x = 0, 0.10, and 0.15 heterostructures, rhombohedral splitting of the $Bi_{1-x}La_xFeO_3$ 203_c-diffraction peak was clearly observed, confirming a rhombohedral structure. The splitting between the $\bar{2}03_c$- and 203_c-diffraction peaks due to the multivariant domain structure yields the rhombohedral angle $\beta = \tan^{-1}\left(\frac{\Delta q_z/2}{q_x}\right)$,[43,51,52] where Δq_z is the difference of the reciprocal value of $\bar{2}03_c$- and 203_c-diffraction peaks in the out-of-plane direction and q_x is the reciprocal value in the in-plane direction. A summary of the in-plane and out-of-plane lattice parameters (calculated by projecting the off-axis peaks to the in-plane and out-of-plane orientations) and the rhombohedral angle (calculated from the equation above) is provided [Fig. 4(e)]. The out-of-plane lattice parameters are found to decrease with increasing lanthanum substitution, which is consistent with the X-ray line scans [Fig. 2(a)]. For heterostructures with x ≤ 0.15, the crystal structure remains rhombohedral (consistent with previous reports), and the rhombohedral angle decreases with increasing lanthanum substitution [as illustrated for the x = 0 [Fig. 4(f)], 0.1 [Fig. 4(g)], and 0.15 [Fig. 4(h)] heterostructures].[51] For the x = 0.27 heterostructures, the rhombohedral splitting reduces to zero [Fig. 4(i)], implying a change to an orthorhombic phase.[51]

Thus, it is possible to calculate the actual π along the polarization direction (i.e., the rhombohedral $\langle 111 \rangle$) using the rhombohedral angles [Fig. 4(e)] and out-of-plane π for heterostructures with various lanthanum contents, as the π measured in our devices was only the out-of-plane component [Fig. 4(j)]. A slight increase in the pyroelectric response was seen for the x = 0.10 heterostructures, and a pyroelectric response anomaly was
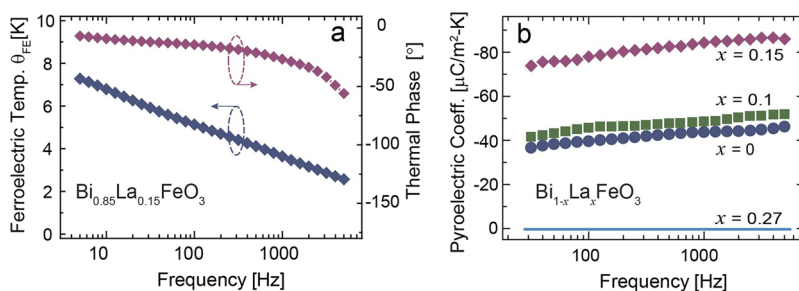

FIG. 3. (a) Temperature oscillation (θ_{FE}, left axis) and thermal phase (right axis) in the ferroelectric layer as a function of heating current frequency as illustrated for the x = 0.15 heterostructures. (b) Pyroelectric coefficient of the various $Bi_{1-x}La_xFeO_3$ heterostructures as a function of heating current frequency at zero dc bias.
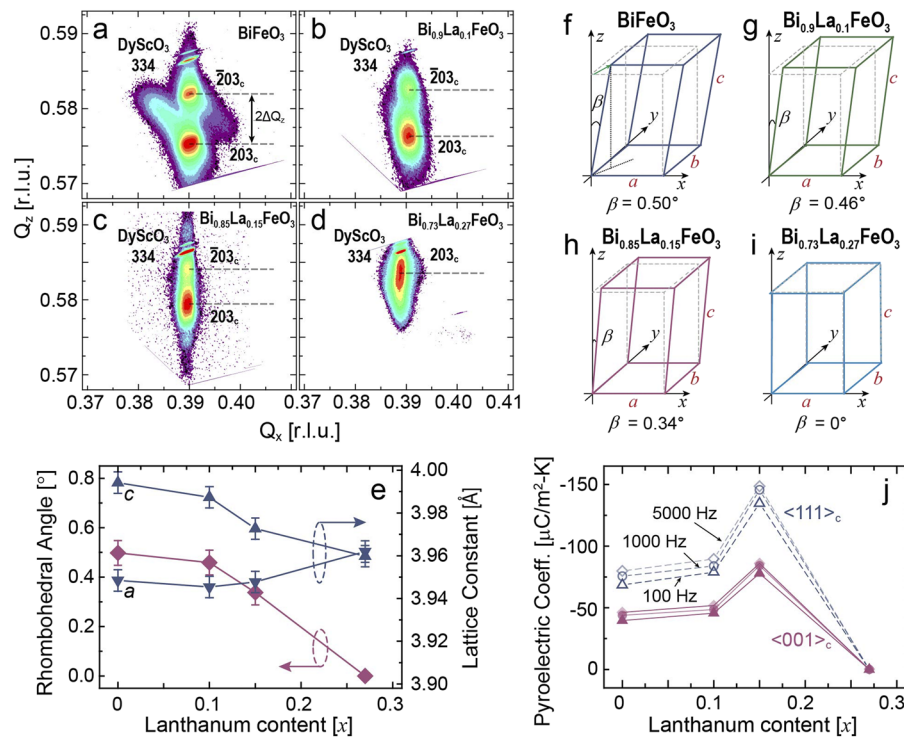
FIG. 4. Off-axis RSM studies about the pseudocubic 203_c/$\bar{2}03_c$- and 334-diffraction conditions of the films and substrates for the (a) x = 0, (b) x = 0.10, (c) x = 0.15, and (d) x = 0.27 heterostructures showing that the splitting of the 203_c- and $\bar{2}03_c$-diffraction peaks decreases and vanishes with increasing lanthanum content. (e) Extracted rhombohedral angle (left axis) as well as the in-plane (a) and out-of-plane (c) lattice constants (right axis) as a function of lanthanum content. Schematic of the evolution of the crystal structure for the (f) x = 0, (g) x = 0.10, (h) x = 0.15, and (i) x = 0.27 heterostructures showing that the structure becomes more orthorhombic-like with increasing lanthanum content. (j) Measured pyroelectric coefficient for the various heterostructures (x = 0, 0.10, and 0.15) in the out-of-plane ⟨001⟩ orientation and calculated pyroelectric coefficient along the ⟨111⟩ polarization axes using the unit-cell structure obtained from the RSM studies as a function of lanthanum content. Note that, for the x = 0.27 heterostructures, RSM studies indicate that the films are paraelectric, and thus, we denote the pyroelectric coefficient to be zero.

observed for the x = 0.15 heterostructures which is accompanied by an increase in dielectric permittivity. Thus, it is possible to conclude that the enhancement of the pyroelectric response does not result from a structural transition from rhombohedral to orthorhombic symmetry wherein the polarization direction rotates from the ⟨111⟩ to the ⟨001⟩ so that the out-of-plane projection of the polarization increases significantly without having any change in the magnitude of π. But this does confirm that proximity to other types of structural-phase transitions can, in fact, be used to enhance the room temperature pyroelectric response of materials—in this case, the chemically induced structural phase boundary gives rise to pyroelectric responses that are comparable to those measured along the polarization direction in other lower T_C ferroelectrics.

Having established that polarization rotation corresponding to a structural evolution is not responsible for the majority of the enhancement, we proceed to complete temperature-dependent electrical measurements to probe the evolution of T_C with lanthanum substitution. Temperature- and frequency-dependent dielectric permittivity data were taken for the BiFeO₃ and Bi₀.₀₈₅La₀.₁₅FeO₃ heterostructures [Fig. 5(a)] and the supplementary material, Fig. S4(a)]. Temperature-dependence of the dielectric loss is also provided [supplementary material, Figs. S4(b) and S5]. As expected, the

dielectric response of the x = 0.15 heterostructures is found to be strongly temperature-dependent. With increasing temperature, there is a rapid increase in the dielectric permittivity by ∼100% from 300 K to 550 K for the x = 0.15 heterostructures, while the dielectric permittivity of the x = 0 heterostructures only increases by ∼22% for the same temperature range. These data suggest that T_C of the x = 0.15 heterostructures is considerably reduced relative to that of the x = 0 heterostructures. Such a trend could also be visualized by the schematic of the $Bi_{1-x}La_xFeO_3$ phase diagram [Fig. 5(b)] where the temperature for the ferroelectric-to-paraelectric phase transition is systematically brought down upon increasing the lanthanum content. The red squares [Fig. 5(b)] are experimental data for bulk $Bi_{1-x}La_xFeO_3$ obtained from differential thermal analysis and thermogravimetry,[25] which are consistent with implications from our temperature-dependent dielectric permittivity data that a lowering of T_C could be achieved via lanthanum substitution. It should also be noted that the dielectric permittivity increases by ∼150% when the lanthanum content is increased from x = 0 to 0.15. With the same chemistry change, however, the magnitude of the pyroelectric coefficient increases from −43 to −85 μC/m² K; thus, the total energy harvesting power is increased by ∼55%, which confirms the effectiveness of rare-earth element substitution for
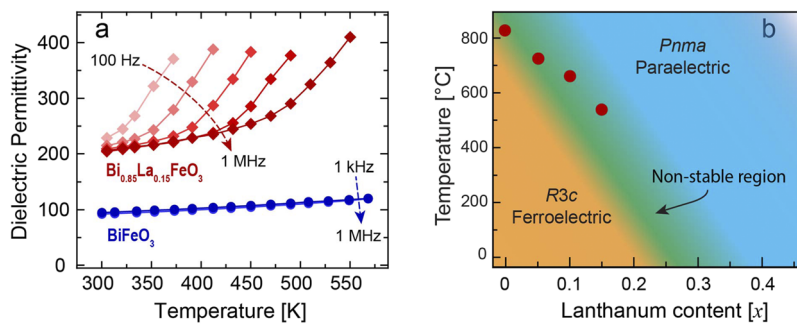
FIG. 5. (a) Temperature-dependence of the dielectric permittivity indicating a more rapid increase in the dielectric permittivity in x = 0.15 heterostructures (red data) than in that of x = 0 heterostructures (blue data). (b) Schematic of the phase diagram of the $Bi_{1-x}La_xFeO_3$ system indicating the paraelectric, ferroelectric, and nonstable regimes as a function of temperature and lanthanum content (red circles are experimental data for T_C of bulk $Bi_{1-x}La_xFeO_3$ taken from Ref. 25, determined by differential thermal analysis and thermogravimetry).

potential energy conversion applications.[45] Moreover, lanthanum-substitution also improves the insulating nature of $BiFeO_3$, which could potentially reduce the noise in the imaging and thermal sensing applications.[45]

In summary, the influence of isovalent substitution in $Bi_{1-x}La_xFeO_3$ thin films on the pyroelectric response was studied. First, we measured the pyroelectric response of $BiFeO_3$ as a function of frequency at room temperature. From there, we showed that the pyroelectric response is increased by ~100% with 15% lanthanum substitution. RSM studies showed that while there was a slight change in the rhombohedral angle with lanthanum substitution, all heterostructures remained rhombohedral for x ≤ 0.15. For x > 0.20, the material transitions to orthorhombic and paraelectric phases. In turn, it was shown that the increase in the pyroelectric response resulted not from the polarization contraction in the rhombohedral direction but due to a reduction in the Curie temperature with lanthanum substitution. Overall, this work provides a route toward enhancing pyroelectric properties of materials by engineering the Curie temperature and motivates the exploration of other pyroelectric materials to further improve their electrothermal susceptibilities wherein a combination of the ferroelastic domain wall,[14,15] ferroelectric multilayers,[53] and the composition-graded structure[54,55] can be applied.

SUPPLEMENTARY MATERIAL

See the supplementary material for additional characterization including dielectric permittivity as a function of applied field, loss tangent as a function of frequency, the temperature oscillations and thermal phase in the ferroelectric heterostructures, and temperature-dependent dielectric permittivity and loss tangent.

ACKNOWLEDGMENTS

REFERENCES

[1] R. W. Whatmore, Rep. Prog. Phys. **49**, 1335 (1986).
[2] R. W. Whatmore, Ferroelectrics **118**, 241 (1991).
[3] S. Pandya, J. Wilbur, J. Kim, R. Gao, A. Dasgupta, C. Dames, and L. W. Martin, Nat. Mater. **17**, 432 (2018).
[4] X. Li, S.-G. Lu, X.-Z. Chen, H. Gu, X. Qian, and Q. M. Zhang, J. Mater. Chem. C **1**, 23 (2013).
[5] C. R. Bowen, J. Taylor, E. LeBoulbar, D. Zabek, A. Chauhan, and R. Vaish, Energy Environ. Sci. **7**, 3836 (2014).
[6] S. P. Alpay, J. Mantese, S. Trolier-McKinstry, Q. Zhang, and R. W. Whatmore, MRS Bull. **39**, 1099 (2014).
[7] S. Pandya, G. Velarde, L. Zhang, J. D. Wilbur, A. Smith, B. Hanrahan, C. Dames, and L. W. Martin, NPG Asia Mater. **11**, 26 (2019).
[8] G. Sebald, D. Guyomar, and A. Agbossou, Smart Mater. Struct. **18**, 125006 (2009).
[9] L. W. Martin and A. M. Rappe, Nat. Rev. Mater. **2**, 16087 (2016).
[10] L. W. Martin, Y.-H. Chu, and R. Ramesh, Mater. Sci. Eng., R **68**, 89 (2010).
[11] M. Brahlek, A. Sen Gupta, J. Lapano, J. Roth, H.-T. Zhang, L. Zhang, R. Haislmaier, and R. Engel-Herbert, Adv. Funct. Mater. **28**, 1702772 (2018).
[12] S. Pandya, J. D. Wilbur, B. Bhatia, A. R. Damodaran, C. Monachon, A. Dasgupta, W. P. King, C. Dames, and L. W. Martin, Phys. Rev. Appl. **7**, 034025 (2017).
[13] B. Bhatia, A. R. Damodaran, H. Cho, L. W. Martin, and W. P. King, J. Appl. Phys. **116**, 194509 (2014).
[14] J. Karthik, J. C. Agar, A. R. Damodaran, and L. W. Martin, Phys. Rev. Lett. **109**, 257602 (2012).
[15] S. Pandya, G. A. Velarde, R. Gao, A. S. Everhardt, J. D. Wilbur, R. Xu, J. T. Maher, J. C. Agar, C. Dames, and L. W. Martin, Adv. Mater. **31**, 1803312 (2019).
[16] S. Pandya, G. Velarde, L. Zhang, and L. W. Martin, Phys. Rev. Mater. **2**, 124405 (2018).
[17] S. W. Smith, A. R. Kitahara, M. A. Rodriguez, M. D. Henry, M. T. Brumbach, and J. F. Ihlefeld, Appl. Phys. Lett. **110**, 072901 (2017).
[18] S. T. Liu, J. D. Zook, and D. Long, Ferroelectrics **9**, 39 (1975).
[19] S. T. Liu and J. D. Zook, Ferroelectrics **7**, 171 (1974).
[20] G. A. Samara, Phys. Rev. **151**, 378 (1966).
[21] I. C. Infante, S. Lisenkov, B. Dupé, M. Bibes, S. Fusil, E. Jacquet, G. Geneste, S. Petit, A. Courtial, J. Juraszek et al., Phys. Rev. Lett. **105**, 057601 (2010).
[22] J. Ravez, Phase Transitions **33**, 53 (1991).
[23] S. T. Liu, J. D. Heaps, and O. N. Tufte, Ferroelectrics **3**, 281 (1972).
[24] B. Fan, G. Yang, M.-Y. Li, P. Liu, S. Qiu, M. Shen, H. Liu, G. Zhang, Q. Wang, and S. Jiang, Ceram. Int. **44**, 8270 (2018).

[25] H. Uchida, R. Ueno, H. Funakubo, and S. Koda, J. Appl. Phys. **100**, 014106 (2006).

[26] B. Xu, D. Wang, J. Íñiguez, and L. Bellaiche, Adv. Funct. Mater. **25**, 552 (2015).

[27] D. C. Arnold, IEEE Trans. Ultrason., Ferroelectr., Freq. Control **62**, 62 (2015).

[28] I. Levin, M. G. Tucker, H. Wu, V. Provenzano, C. L. Dennis, S. Karimi, T. Comyn, T. Stevenson, R. I. Smith, and I. M. Reaney, Chem. Mater. **23**, 2166 (2011).

[29] D. Sando, A. Barthélémy, and M. Bibes, J. Phys.: Condens. Matter **26**, 473201 (2014).

[30] D. Kan, V. Anbusathaiah, and I. Takeuchi, Adv. Mater. **23**, 1765 (2011).

[31] S. Fujino, M. Murakami, V. Anbusathaiah, S.-H. Lim, V. Nagarajan, C. J. Fennie, M. Wuttig, L. Salamanca-Riba, and I. Takeuchi, Appl. Phys. Lett. **92**, 202904 (2008).

[32] L. You, F. Zheng, L. Fang, Y. Zhou, L. Z. Tan, Z. Zhang, G. Ma, D. Schmidt, A. Rusydi, L. Wang et al., Sci. Adv. **4**, eaat3438 (2018).

[33] Y. B. Yao, W. C. Liu, and C. L. Mak, J. Alloys Compd. **527**, 157 (2012).

[34] Y. H. Chu, L. W. Martin, Q. Zhan, P. L. Yang, M. P. Cruz, K. Lee, M. Barry, S. Y. Yang, and R. Ramesh, Ferroelectrics **354**, 167 (2007).

[35] J. T. Heron, D. G. Schlom, and R. Ramesh, Appl. Phys. Rev. **1**, 021303 (2014).

[36] L. W. Martin and D. G. Schlom, Curr. Opin. Solid State Mater. Sci. **16**, 199 (2012).

[37] Y. Yao, B. Ploss, C. L. Mak, and K. H. Wong, Appl. Phys. A **99**, 211 (2010).

[38] Y. Yao, W. Liu, Y. Chan, C. Leung, C. Mak, and B. Ploss, Int. J. Appl. Ceram. Technol. **8**, 1246 (2011).

[39] Y. V. Shaldin, S. Matyjasik, and A. A. Bush, Crystallogr. Rep. **52**, 123 (2007).

[40] C.-H. Chiu, W.-I. Liang, C.-W. Huang, J.-Y. Chen, Y.-Y. Liu, J.-Y. Li, C.-L. Hsin, Y.-H. Chu, and W.-W. Wu, Nano Energy **17**, 72 (2015).

[41] G. W. Pabst, L. W. Martin, Y.-H. Chu, and R. Ramesh, Appl. Phys. Lett. **90**, 072902 (2007).

[42] L. R. Dedon, S. Saremi, Z. Chen, A. R. Damodaran, B. A. Apgar, R. Gao, and L. W. Martin, Chem. Mater. **28**, 5952 (2016).

[43] Z. H. Chen, A. R. Damodaran, R. Xu, S. Lee, and L. W. Martin, Appl. Phys. Lett. **104**, 182908 (2014).

[44] S. Jachalke, E. Mehner, H. Stöcker, J. Hanzig, M. Sonntag, T. Weigel, T. Leisegang, and D. C. Meyer, Appl. Phys. Rev. **4**, 021303 (2017).

[45] P. Muralt, Rep. Prog. Phys. **64**, 1339 (2001).

[46] P. W. Haycock and P. D. Townsend, Appl. Phys. Lett. **48**, 698 (1986).

[47] B. Ploss and S. Bauer, Sens. Actuators, A **26**, 407 (1991).

[48] A. M. Glass, Phys. Rev. **172**, 564 (1968).

[49] J. F. Ihlefeld, C. M. Folkman, S. H. Baek, G. L. Brennecka, M. C. George, J. F. Carroll III, and C. B. Eom, Appl. Phys. Lett. **97**, 262904 (2010).

[50] G. Catalan and J. F. Scott, Adv. Mater. **21**, 2463 (2009).

[51] Y. H. Chu, Q. Zhan, C.-H. Yang, M. P. Cruz, L. W. Martin, T. Zhao, P. Yu, R. Ramesh, P. T. Joseph, I. N. Lin et al., Appl. Phys. Lett. **92**, 102909 (2008).

[52] B.-K. Jang, J. H. Lee, K. Chu, P. Sharma, G.-Y. Kim, K.-T. Ko, K.-E. Kim, Y.-J. Kim, K. Kang, H.-B. Jang et al., Nat. Phys. **13**, 189 (2017).

[53] M. T. Kesim, J. Zhang, S. P. Alpay, and L. W. Martin, Appl. Phys. Lett. **105**, 052901 (2014).

[54] R. V. K. Mangalam, J. C. Agar, A. R. Damodaran, J. Karthik, and L. W. Martin, ACS Appl. Mater. Interfaces **5**, 13235 (2013).

[55] J. Karthik, R. V. K. Mangalam, J. C. Agar, and L. W. Martin, Phys. Rev. B **87**, 024111 (2013).